JOURNAL OF ASIAN CERAMIC SOCIETIES
2021, VOL. 9, NO. 3, 1147–1153
https://doi.org/10.1080/21870764.2021.1944556

Crystal Structures and Electronic States of High-Pressure-Synthesized (1-*x*)$PbVO_3$-*x*$BiCrO_3$ Solid Solutions

Hajime Yamamoto[a], Haruna Aizawa[a], Ikuya Yamada[b], Kaoru Toda[a], Atsushi Tanaka[b], Masaki Azuma[c,d], Yuki Sakai[c,d], Takumi Nishikubo[c] and Hiroyuki Kimura[a]

[a]Institute of Multidisciplinary Research for Advanced Materials, Tohoku University, Sendai, Japan; [b]Department of Materials Science, Graduate School of Engineering, Osaka Prefecture University, Osaka, Japan; [c]Laboratory for Materials and Structures, Tokyo Institute of Technology, Yokohama, Japan; [d]Kanagawa Institute of Industrial Science and Technology, Kanagawa, Japan

ABSTRACT

Electronic states in solid-solution transition metal oxides may differ from those in their parent compounds, and this results in interesting electronic properties. In this study, the valence states and electronic properties of solid solutions of (1 − *x*)$PbVO_3$− *x*$BiCrO_3$ are reported. The solid solutions are successfully synthesized under high-pressure and high-temperature conditions of 5 GPa or 7 GPa and 1273 K, respectively. A change in the crystal structure from centrosymmetric monoclinic (*C*2/*c*), as in $BiCrO_3$, to polar tetragonal (*P*4*mm*), as in $PbVO_3$, is observed. A tetragonal-to-cubic phase transition, which results in a negative thermal expansion, was observed in 7/8$PbVO_3$-1/8$BiCrO_3$ at approximately 700 K. X-ray absorption spectroscopy and magnetic studies reveal that the Cr and V atoms are in the valence states 3+ and 4+, respectively, which are the same as those of the parent compounds. Thus, it was concluded that the valence state of V^{4+}/Cr^{3+} and the electron localization in the (1 − *x*)$PbVO_3$− *x*$BiCrO_3$ solid solutions are considerably robust.

ARTICLE HISTORY
Received 28 April 2021
Accepted 15 June 2021

KEYWORDS
High-pressure synthesis; solid solution; valence state; magnetism

1. Introduction

Valence states in solid solutions are sometimes different from those in their parent compounds, because of the difference in the energy of the valence orbitals of the constituent ions, that is, the electronegativity. High-pressure synthesis is a powerful tool for preparing solid solutions because the applied pressure prevents ion desorption due to Le Chatelier's principle. Recently, we reported a high-pressure synthesis and elucidated the valence states of perovskite-type $PbVO_3$ – $BiCoO_3$ solid solutions [1]. An intermetallic charge transfer between vanadium and cobalt ions, that is, $V^{4+} + Co^{3+} \rightarrow V^{5+} + Co^{2+}$, was observed, which resulted in a polar-to-nonpolar structural transition and a large volume shrinkage.

Perovskite-type $PbVO_3$ possesses a $PbTiO_3$-type tetragonal distortion [2,3]. The *c*/*a* ratio (tetragonality) reaches 1.23, which is considerably higher than that of $PbTiO_3$. Both the divalent lead ion (*A*-site) and the tetravalent vanadium ion (*B*-site) contribute to the enhancement of the tetragonal distortion. This tetragonal structure is stabilized by the strong covalency of the Pb–O bonds and the stereochemical activity of the $6s^2$ lone pairs [4]. Furthermore, the Jahn–Teller effect of V^{4+} ($3d^1$) contributes to strengthening the distortion [5,6]. The t_{2g} orbital degeneracy is lifted in the square pyramidal geometry, splitting into stabilized $3d_{xy}$ and destabilized $3d_{yz}$ and $3d_{zx}$ orbitals, as shown in Figure 1. A single d-electron occupies the $3d_{xy}$ orbital, which stabilizes the distortion.

At room temperature, perovskite-type $BiCrO_3$ has a centrosymmetric monoclinic symmetry with the space group *C*2/*c* (Figure 1)[7–9], which is transformed into a $GdFeO_3$-type orthorhombic structure with the *Pnma* space group at 420 K [8,10,11]. The valence state is $Bi^{3+}Cr^{3+}O_3$, which is not Jahn–Teller active [12]. $BiCrO_3$ undergoes an antiferromagnetic transition below the Néel temperature, T_N, of ~110 K [7]. Spin reorientation occurs at approximately 80 K, increasing the magnetization caused by the Dzyaloshinskii–Moriya interaction [8]. Notably, a related compound $PbCrO_3$, which also possesses a trivalent chromium ion [13], has a valence state of $Pb^{2+}_{0.5}Pb^{4+}_{0.5}Cr^{3+}O_3$, indicating that the Pb-6s and Cr-3d levels are close. Moreover, a pressure-induced intermetallic charge transfer from $Pb^{2+}_{0.5}Pb^{4+}_{0.5}Cr^{3+}O_3$ to $Pb^{2+}Cr^{4+}O_3$ was observed at 2.5 GPa.

Based on this context, we investigated the valence state of (1 − *x*)$PbVO_3$− *x*$BiCrO_3$ solid solutions for the following reasons. First, an intermetallic charge transfer and a complex valence state can be expected because of the close energy of the valence orbitals of chromium, vanadium, and lead ions. Second, an insulator-to-metal transition similar to that of $PbV_{1-x}Cr_xO_3$

CONTACT Hajime Yamamoto Email hajime.yamamoto.a2@tohoku.ac.jp Institute of Multidisciplinary Research for Advanced Materials, Tohoku University, Sendai, Japan
Supplemental data for this article can be accessed here.

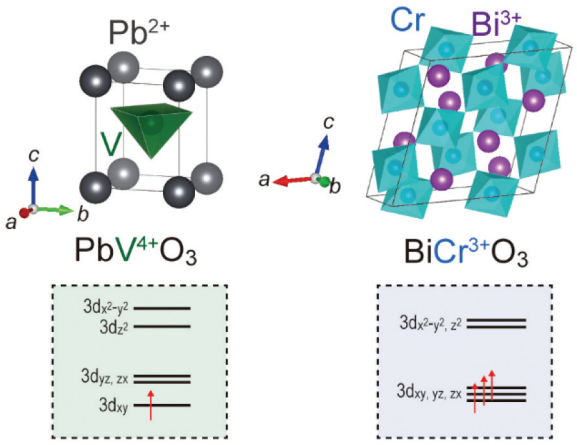

Figure 1. Schematic images of the crystal structures and electronic configurations of the 3d transition metals of $PbVO_3$ (left) and $BiCrO_3$ (right).

may occur [14]. Herein, the evolution of the crystal structure, valence state, and electronic properties of $(1-x)PbVO_3-xBiCrO_3$ (x = 1/8 − 7/8) solid solutions were studied. Solid solutions were synthesized using a high-pressure and high-temperature (HP–HT) method. The crystal structure was observed to change from polar tetragonal ($PbVO_3$ side) to centrosymmetric monoclinic ($BiCrO_3$ side). X-ray absorption spectroscopy (XAS) and magnetic susceptibility measurements confirmed that all the compounds had the valence states V^{4+} and Cr^{3+}, which were the same as those of the end members. The semiconductive behavior of these compounds is attributed to these valence states. The weak ferromagnetism was systematically suppressed by increasing the $PbVO_3$ content, which may be attributed to a change in the spin orientation. The pressure dependence of electrical resistivity in the $4/8PbVO_3$-$4/8BiCrO_3$ sample demonstrates the robustness of the V^{4+}–Cr^{3+} valence state and the electron localization. A tetragonal-to-cubic phase transition, which may result in an insulator-to-metal transition, was observed in $7/8PbVO_3$-$1/8BiCrO_3$. This transition was accompanied by a negative thermal expansion.

2. Experimental section

Polycrystalline samples of $(1-x)PbVO_3-xBiCrO_3$ (x = 2/8, 3/8, 4/8, 5/8, 6/8, and 7/8) were synthesized from stoichiometric mixtures of PbO, Bi_2O_3, V_2O_3, V_2O_5, and Cr_2O_3 packed in a Pt capsule at 5 GPa and 1273 K for 30 min using a cubic anvil cell-type high-pressure apparatus. A $7/8PbVO_3$-$1/8BiCrO_3$ (x = 1/8) sample was synthesized at 7 GPa and 1273 K for 30 min using a Walker-type high-pressure apparatus. Synchrotron X-ray diffraction (SXRD) measurements were conducted on BL19B2 and BL02B2, SPring-8, Japan, at a wavelength of λ = 0.42 Å. The SXRD data were analyzed via the Rietveld method using the RIETAN-FP program [15]. Negligible amounts of impurities, including $Pb_3V_2O_8$ and Bi_2O_3, were observed, except in case of the $6/8PbVO_3$-$2/8BiCrO_3$ sample. The crystal structures were drawn using the VESTA program [16]. Soft XAS measurements of the $L_{2,3}$ edge of Cr for all the samples and $BiCrO_3$ were conducted at room temperature using the total electron yield method at the BL12, SAGA-LS, Kyushu Synchrotron Light Research Center. The temperature dependence of the magnetic susceptibility of all samples with x = 1/8–5/8 was measured using a superconducting quantum interference device magnetometer (Quantum Design, MPMS). The temperature (two-probe method) and pressure dependence (quasi-four-probe method) of the electrical resistivity of the $4/8PbVO_3$-$4/8BiCrO_3$ sample was measured using a multimeter (Keithley 2100), a cryostat, and a high-pressure apparatus.

3. Results and discussion

Figure 2 **(a)–(f)** show the SXRD patterns of the $(1-x)PbVO_3-xBiCrO_3$ solid solutions. Perovskite-type phases were obtained for all the samples. Space groups and crystal structures were successfully determined for $1/8PbVO_3$-$7/8BiCrO_3$ and $7/8PbVO_3$-$1/8BiCrO_3$ samples, as shown in Figure 3. However, in the other composites, peak overlaps, as explained below, and the occurrence of peak broadening, which

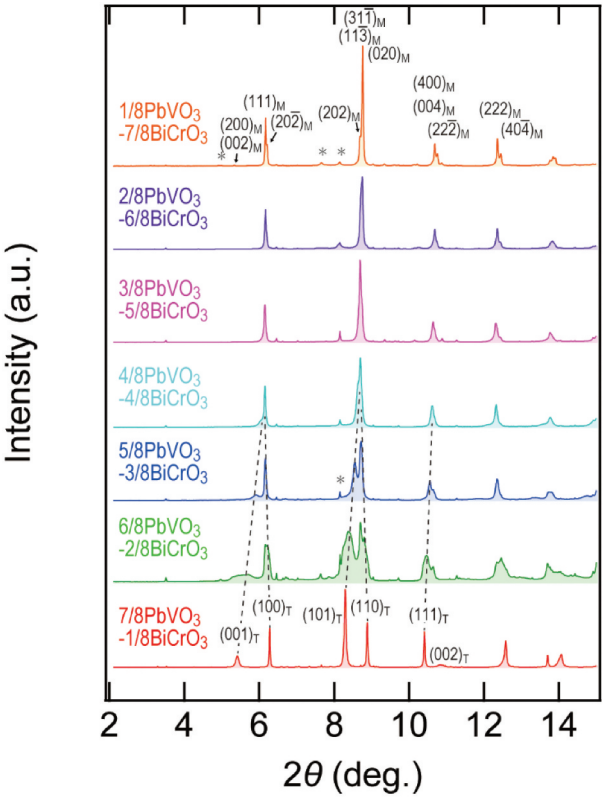

Figure 2. Synchrotron X-ray diffraction patterns of the $(1-x)PbVO_3$–$xBiCrO_3$ samples. M and T represent the monoclinic and tetragonal phases, respectively; the asterisks (*) denote the impurity phases; and the dashed lines show the change in the peaks of the tetragonal phase.

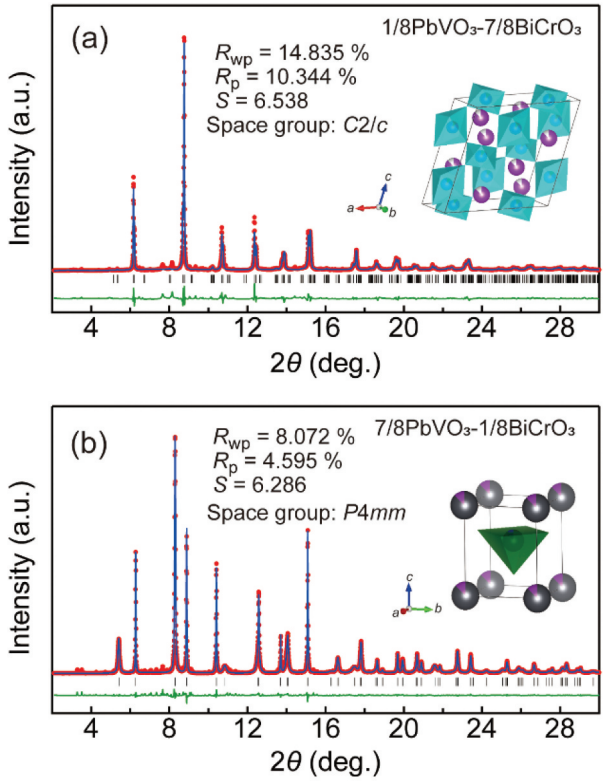

Figure 3. Rietveld refinement results for $1/8PbVO_3$–$7/8BiCrO_3$ and $7/8PbVO_3$–$1/8BiCrO_3$. Observed (red points) and calculated (blue line) SXRD patterns, and their difference (green line) for **(a)** $1/8PbVO_3$-$7/8BiCrO_3$ and **(b)** $7/8PbVO_3$-$1/8BiCrO_3$ at room temperature. The tick marks correspond to the position of Bragg reflections of each perovskite phase. Crystal structures shows the obtained one.

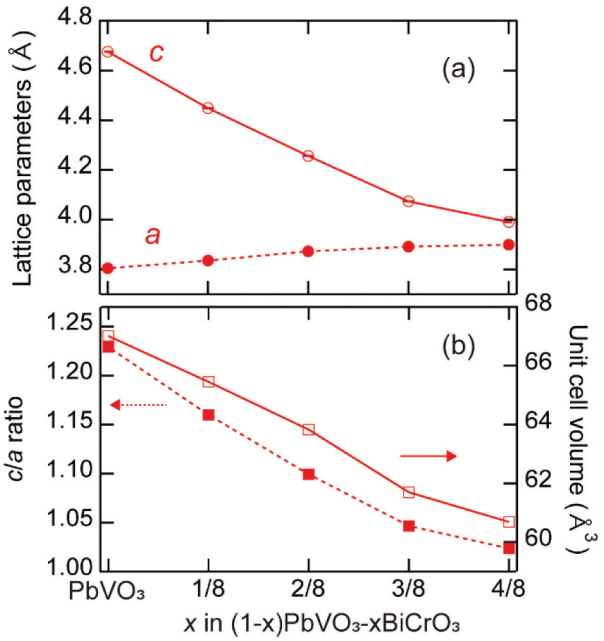

Figure 4. Evolution of the lattice parameters of the tetragonal phase of the $(1 - x)PbVO_3$– $xBiCrO_3$ solid solutions; (a) lattice parameters (*c*- and *a*- axis lengths); (b) *c*/*a* ratio and unit cell volume. The lattice parameters of $PbVO_3$ were obtained from Ref. 18.

may result from local disorder [17], hindered good agreement from crystal structure refinement. The lattice parameters and crystal structure parameters are shown in Figure S1 and Tables S1–S4. A centrosymmetric monoclinic (*C*2/*c*) phase, which is the same as that in $BiCrO_3$, was observed in the x = 7/8–6/8 samples. The monoclinic phase seems to be preserved in the samples with x = 5/8–3/8; however, because of peak overlaps, their lattice parameters could not be precisely determined. No superlattice reflection indicating cation ordering was observed, even in the $4/8PbVO_3$–$4/8BiCrO_3$ sample. A polar tetragonal (*P*4*mm*) phase was also observed in the $4/8PbVO_3$–$4/8BiCrO_3$ and $3/8PbVO_3$–$5/8BiCrO_3$ samples. The fraction of the tetragonal phase was found to increase with increasing $PbVO_3$ content, and the $7/8PbVO_3$–$1/8BiCrO_3$ sample possessed only the tetragonal structure. Figure 4 shows the evolution of the lattice parameters of the tetragonal phase, and Table S2 summarizes the corresponding numerical values. The *c*/*a* ratio systematically increased toward the $PbVO_3$ edge, which can be ascribed to an increase in the fraction of the Jahn–Teller active tetravalent vanadium ion [18]. The $6/8PbVO_3$–$2/8BiCrO_3$ samples showed an abnormal peak broadening, even the samples synthesized at 7 GPa (Figure S2). This broadening may result from composition fluctuations owing to phase separation. While an additional phase was observed in the $(1 - x)PbVO_3$– $xBiCoO_3$ solid solutions, no additional changes were observed in the present system [1].

Figure 5 shows the XAS spectra of the Cr $L_{2,3}$ edge of $BiCrO_3$ and all the synthesized $(1 - x)PbVO_3$– $xBiCrO_3$

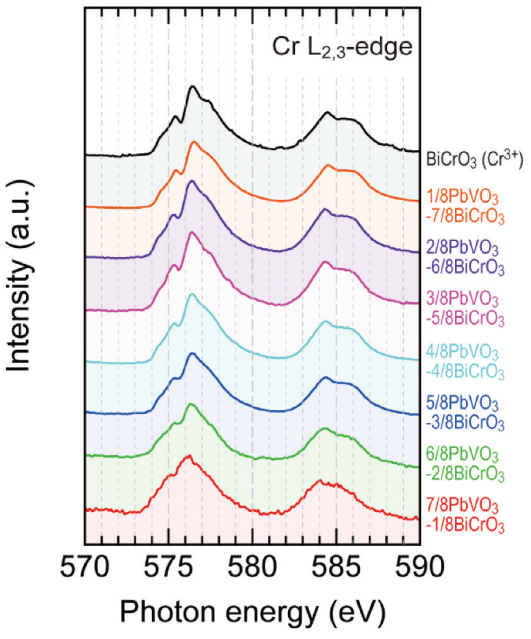

Figure 5. X-ray absorption spectra of the Cr $L_{2,3}$ edge for $BiCrO_3$ (black), $1/8PbVO_3$–$7/8BiCrO_3$ (orange), $2/8PbVO_3$–$6/8BiCrO_3$ (purple), $3/8PbVO_3$–$5/8BiCrO_3$ (pink), $4/8PbVO_3$–$4/8BiCrO_3$ (turquoise), $5/8PbVO_3$–$3/8BiCrO_3$ (blue), $6/8PbVO_3$–$2/8BiCrO_3$ (green), and $7/8PbVO_3$–$1/8BiCrO_3$ (red).

solid solutions. White lines at approximately 576 eV (L_3 edge) and 584 eV (L_2 edge), confirming the presence of the Cr^{3+} state, were observed for the $BiCrO_3$ sample. Similar spectra were obtained for the $(1 - x)PbVO_3 - xBiCrO_3$ samples, indicating that trivalent chromium ions were preserved even after the solid solutions were prepared. To completely determine the valence state and reveal the magnetic properties, the temperature dependence of the magnetic susceptibility was measured for the $(1 - x)PbVO_3$–$xBiCrO_3$ samples with $3/8 \le x \le 7/8$; results are shown in Figure 6 **(a)**–**(e)**. For each sample, an antiferromagnetic transition occurred at approximately 110 K. Clear Curie–Weiss behaviors were observed above 200 K, with an obvious linear behavior in the reciprocal plot (insets of Figure 6 **(a)**–**(e)**). The data in the temperature range of 250–300 K in the reciprocal plots were fitted using the Curie–Weiss law, $\chi^{-1} = H/M = (T - \theta_W)/C$, where C is the Curie constant and θ_W is the Weiss temperature. Table 1 summarizes the obtained and theoretical values. The value of the Curie constant for $1/8PbVO_3$–$7/8BiCrO_3$ was larger than that expected for $Pb^{2+}V^{4+}O_3$–$Bi^{3+}Cr^{3+}O_3$. A similar trend, attributed to the presence of a short-range order, was reported for $BiCrO_3$ [19,20]. The same reason could explain the overestimation of the Weiss temperature. By increasing the $PbVO_3$ content, the Curie constant converged to the theoretical value (Figure S3). Given that the presence of Cr^{3+} was verified by XAS, this result confirms the valence states of $Pb^{2+}V^{4+}O_3$–$Bi^{3+}Cr^{3+}O_3$ for the solid solutions.

The preparation of the solid solution clearly affected the antiferromagnetic properties of the compound. Below the T_N, an increase in the susceptibility of the $1/8PbVO_3$–$7/8BiCrO_3$ sample was observed at 90–100 K, which may correspond to a spin reorientation transition [8,17]. The antiferromagnetic orderings possess weak ferromagnetic components because of the Dzyaloshinskii–Moriya interaction [21]. In $BiCrO_3$, the magnetic moments align along the *b*-axis at 90 K and rotate in the *bc*-plane by ~50° below the spin reorientation temperature (60–80 K) [8]. This reorientation results in a prominent increase in spontaneous magnetization. Interestingly, this anomaly at 90–100 K was suppressed by gradually increasing the $PbVO_3$ content. The remanent magnetization also decreased systematically (Figure 6 **(f)** shows the *M*–*H* curves), which may be attributed to a change in the orientation of the magnetic spin [22]. A theoretical study predicted that

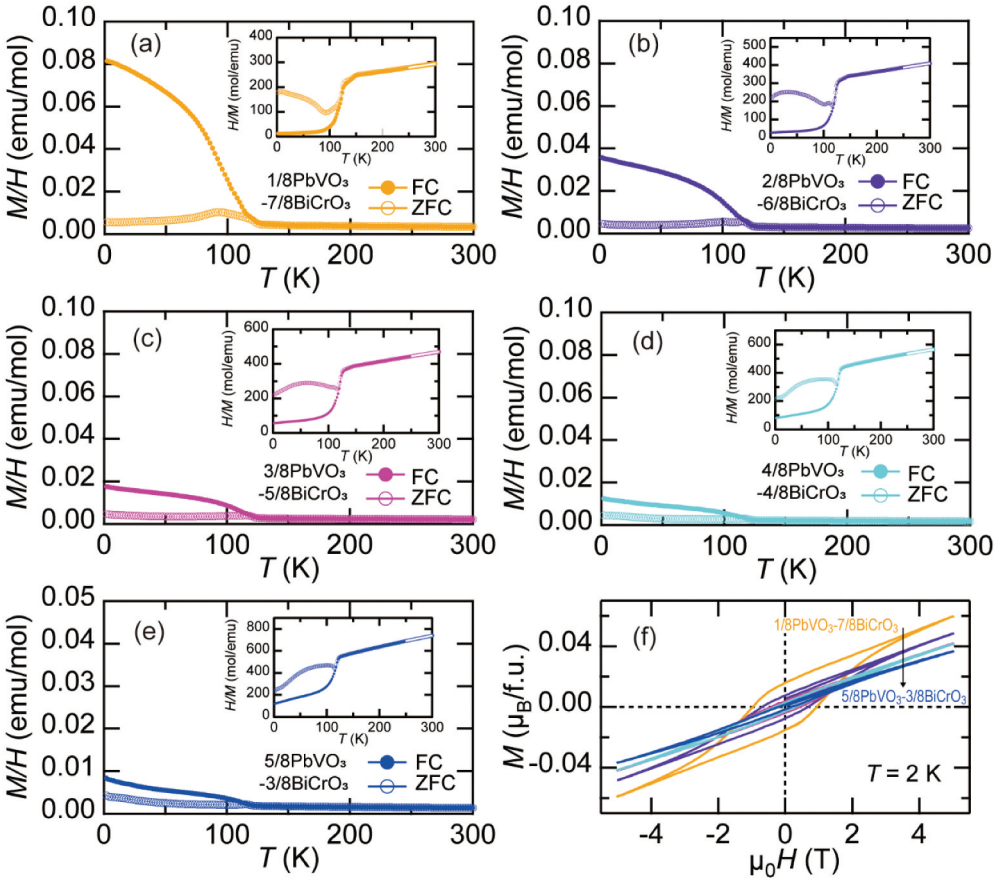

Figure 6. (a)–(e) Temperature dependence of the magnetic susceptibility at a magnetic field of $\mu_0 H = 0.1$ T: (a) $1/8PbVO_3$–$7/8BiCrO_3$, (b) $2/8PbVO_3$–$6/8BiCrO_3$, (c) $3/8PbVO_3$–$5/8BiCrO_3$, (d) $4/8PbVO_3$–$4/8BiCrO_3$, and (e) $5/8PbVO_3$–$3/8BiCrO_3$ samples. FC and ZFC represent field-cooling and zero-field-cooling processes, respectively. The insets provide the reciprocal plots. The white lines between 250 and 300 K (reciprocal plot, FC) feature the results of fitting to the Curie–Weiss law. (f) Magnetic field dependence of the magnetization at $T = 2$ K for all the $(1 - x)PbVO_3$–$xBiCrO_3$ samples.

Table 1. Results of the Curie–Weiss fitting of reciprocal susceptibility (FC) data between 250 and 300 K.

Sample	θ_W* (K)	$C_{exp.}$* (emu K mol^{-1})	$C_{calc.}$* (emu K mol^{-1})
1/8$PbVO_3$ 7/8$BiCrO_3$	−635(14)	3.17(5)	1.69
2/8$PbVO_3$ 6/8$BiCrO_3$	−565(4)	2.11(1)	1.50
3/8$PbVO_3$ 5/8$BiCrO_3$	−620(7)	1.96(2)	1.31
4/8$PbVO_3$ 4/8$BiCrO_3$	−628(7)	1.64(1)	1.12
5/8$PbVO_3$ 3/8$BiCrO_3$	−440(4)	1.00(1)	0.94

*θ_W is the Weiss temperature $C_{exp.}$ and $C_{calc.}$ are the experimental and theoretical Curie constants, respectively. $C_{calc.}$ was expected for the valence state $Pb^{2+}V^{4+}O_3$–$Bi^{3+}Cr^{3+}O_3$.

the combination of highest occupied molecular orbital (HOMO) and lowest unoccupied molecular orbital (LUMO) determines the spin direction [23]. In the case of Cr^{3+} and V^{4+}, HOMO and LUMO are $3d_{xy,yz,zx}$ and $3d_{x^2-y^2,z^2}$ orbitals, respectively, for Cr^{3+}, and both $3d_{xy,yz,zx}$ orbitals for V^{4+}. Neutron diffraction measurements are necessary to reveal the details.

The $(1-x)PbVO_3$–$xBiCrO_3$ samples exhibited Mott insulator features at ambient pressure. As a representative example, the temperature dependence of the electrical resistivity of the 4/8$PbVO_3$ –4/8$BiCrO_3$ sample is shown in Figure 7 **(a)**. The inset shows the lnρ – 1000/T plot. A clear semiconductive behavior was observed. The activation energy obtained from the Arrhenius plot was E_a = 0.28 eV, which is similar to that observed in perovskite-type tetravalent vanadates and trivalent chromates (Mott insulators) [22,24]. The pressure dependence of the electrical resistivity up to 5 GPa was measured because the external field was expected to induce an insulator-to-metal transition or intermetallic charge transfer, as previously observed for $PbVO_3$, $PbCrO_3$, $PbCoO_3$, and $BiNiO_3$ [2,13,25–27]; results are shown in Figure 7 **(b)**. A clear resistivity drop was not observed, indicating that the abovementioned phenomena did not occur up to 5 GPa. Taken together, these results suggest that the valence state of V^{4+}/Cr^{3+} and the electron localization in the $(1-x)PbVO_3$–$xBiCrO_3$ solid solutions are quite robust.

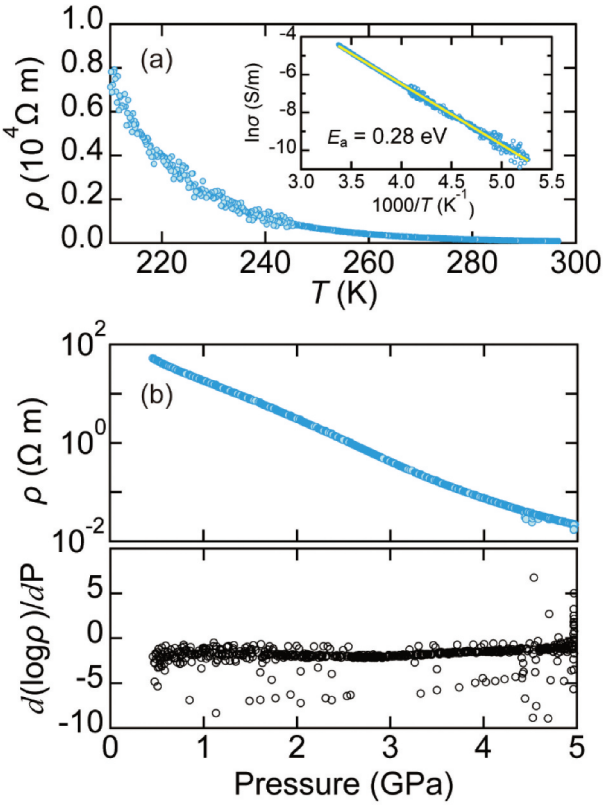

Figure 7. (a) Temperature dependence of the electric resistivity of the 4/8$PbVO_3$–4/8$BiCrO_3$ sample. The inset shows an Arrhenius plot and the result of fitting by the Arrhenius equation $\rho \sim \exp(-E_a/k_BT)$ (yellow line), where E_a is the activation energy and k_B is the Boltzmann constant. (b) Pressure dependence of the electric resistivity of the 4/8$PbVO_3$ –4/8$BiCrO_3$ sample up to 5 GPa at ambient temperature.

A tetragonal-to-cubic phase transition was observed in the 7/8$PbVO_3$-1/8$BiCrO_3$ sample, which was accompanied by a negative thermal expansion. Note that a crystal structure transition was not observed in $PbVO_3$ because the Curie temperature was higher than the decomposition one [2]. Figure 8 shows the SXRD patterns for heating and cooling between 100 and 700 K. A cubic perovskite-type phase appeared at 700 K during heating. The unit cell volume was ~8.0% smaller than that of the tetragonal structure, which could lead to the realization of an excessively high negative thermal expansion. The phase transition was not completed at temperatures up to 700 K. The fraction of the cubic phase decreased with decreasing temperature; however, approximately 16% of the cubic phase remained even at 100 K, as shown in Figure 9. The tetragonal-to-cubic phase transition may be accompanied by an insulator-to-metal transition, as in the case of Cr-substituted $PbVO_3$ [14]. The presence of trivalent chromium ions weakens the Jahn–Teller effect and may introduce electronic itinerancy, which may trigger phase transition in 7/8$PbVO_3$ -1/8$BiCrO_3$.

4. Conclusion

In summary, we reported the evolution of the crystal structures, valence states, and electronic properties of $(1-x)PbVO_3$–$xBiCrO_3$ solid solutions. Solid solutions were synthesized using the HP–HT method. The crystal structures changed from polar tetragonal ($P4mm$, $PbVO_3$ side) to centrosymmetric monoclinic ($C2/c$, $BiCrO_3$ side). A tetragonal-to-cubic phase transition, which may result in an insulator-to-metal transition, was observed at approximately 700 K in 7/8$PbVO_3$-1/8$BiCrO_3$. This transition was accompanied by a negative thermal expansion. XAS and magnetic measurements revealed that the solid solutions have a valence state of $Pb^{2+}V^{4+}O_3$–$Bi^{3+}Cr^{3+}O_3$, which is the same as that of the end members. The

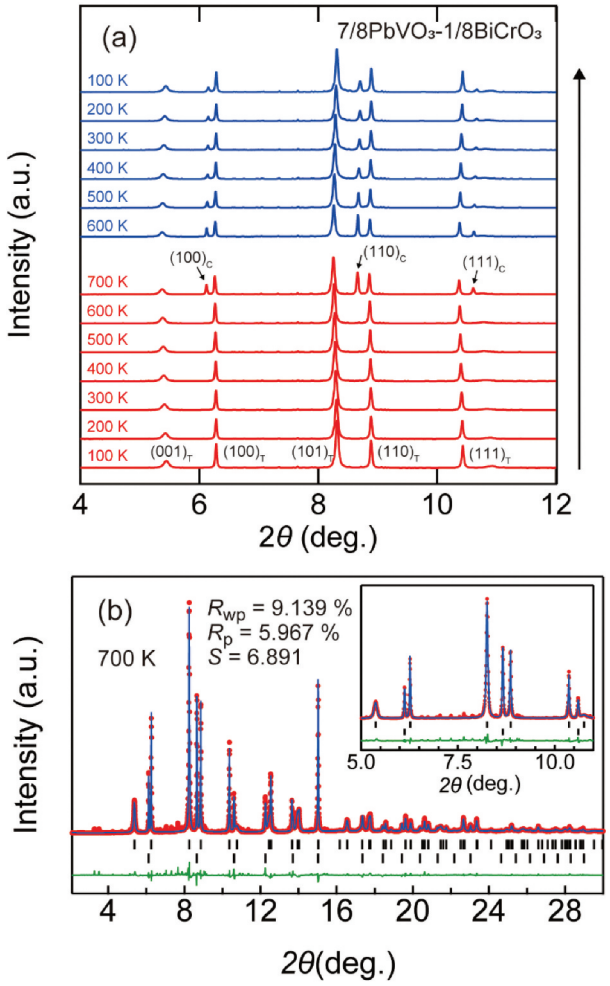

Figure 8. **(a)** Temperature variation of SXRD patterns of $7/8PbVO_3$–$1/8BiCrO_3$ on heating and cooling. C and T represent the cubic and tetragonal phases, respectively. **(b)** Rietveld refinement results for $7/8PbVO_3$–$1/8BiCrO_3$ at 700 K. Observed (red points) and calculated (blue line) SXRD patterns, and their difference (green line) are shown. The tick marks correspond to the position of Bragg reflections of tetragonal (top) and cubic (bottom) phases. Inset shows the magnified pattern. The lattice and structure parameters are shown in **Tables S5** and **S6.**

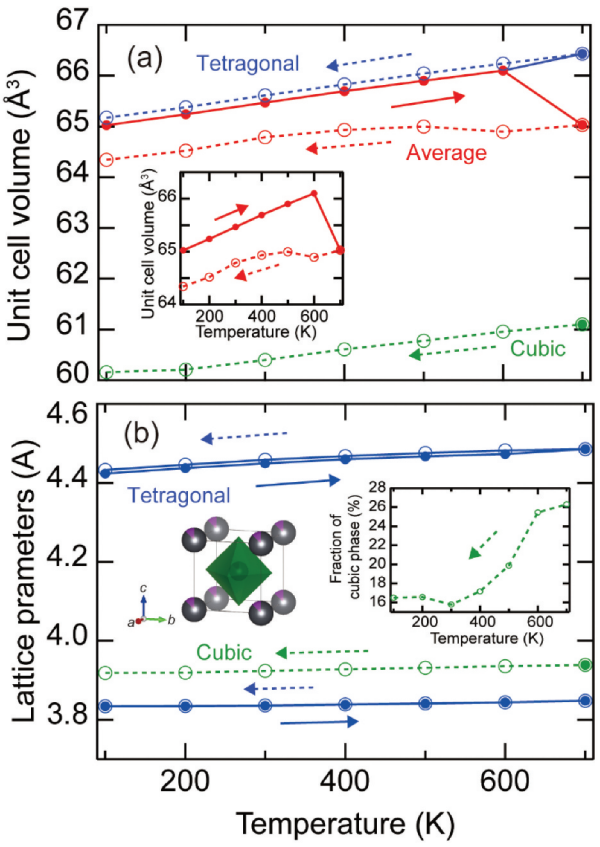

Figure 9. **(a)** Temperature dependence of unit cell volume in $7/8PbVO_3$–$1/8BiCrO_3$ on heating and cooling. Inset shows the magnified view of average unit cell volume. (b) Temperature dependence of lattice parameters in $7/8PbVO_3$–$1/8BiCrO_3$ on heating and cooling. Inset provides the fraction of cubic phase. Crystal structure shows the obtained cubic phase at 700 K.

preparation of the solid solutions might affect the antiferromagnetic orientation of the magnetic spin. The findings of this study could lead to the future development of new functional materials based on solid solutions.

Acknowledgments

The authors thank Dr. Zhao Pan for fruitful discussions, Dr. Eiichi Kobayashi, Mr. Yuta Kato, and Mr. Yuta Kizawa for their support with the XAS measurements, and Dr. Keiichi Osaka for his support with the XRD measurements.

Disclosure of potential conflicts of interest

No potential conflict of interest was reported by the authors.

Funding

This study was partially supported by a Grant-in-Aid for Scientific Research 19K15280 from the Japan Society for the Promotion of Science (JSPS), the Asahi Glass Foundation, Tokuyama Science Foundation, TEPCO Memorial Foundation, and the Collaborative Research Projects of Laboratory for Materials and Structures, Institute of Innovative Research, Tokyo Institute of Technology. This study was conducted with the approval of the Japan Synchrotron Radiation Research Institute (Proposal No. 2020A1773) and SAGA Light Source (proposal No. 2007067F and 2010103F).

ORCID

Hajime Yamamoto http://orcid.org/0000-0001-6327-6803
Ikuya Yamada http://orcid.org/0000-0003-2340-131X

References

[1] Yamamoto H, Toda K, Sakai Y, et al. Emergence of a Cubic Phase Stabilized by Intermetallic Charge Transfer in (1-*x*)$PbVO_3$-*x*$BiCoO_3$ Solid Solutions. Chem Mater. 2020 Aug;32(16):6892–6897.

[2] Belik AA, Azuma M, Saito T, et al. Crystallographic features and tetragonal phase stability of $PbVO_3$, a new member of $PbTiO_3$ family. Chem Mater. 2005 Jan;17(2):269–273.
[3] Shpanchenko RV, Chernaya VV, Tsirlin AA, et al. Synthesis, structure, and properties of new perovskite $PbVO_3$. Chem Mater. 2004 Aug;16(17):3267–3273.
[4] Cohen RE. Origin of ferroelectricity in perovskite oxides. Nature. 1992 Jul;358(6382):136–138.
[5] Oka K, Yamada I, Azuma M, et al. Magnetic ground-state of perovskite $PbVO_3$ with large tetragonal distortion. Inorg Chem. 2008 Aug;47 (16):7355–7359.
[6] Korotin MA, Elfimov IS, Anisimov VI, et al. Exchange interactions and magnetic properties of the layered vanadates CaV_2O_5, MgV_2O_5, CaV_3O_7, and CaV_4O_9. Phys Rev Lett. 1999 Aug;83(7):1387–1390.
[7] Belik AA, Iikubo S, Kodama K, et al. Neutron powder diffraction study on the crystal and magnetic structures of $BiCrO_3$. Chem Mater. 2008 Jun;20 (11):3765–3769.
[8] Darie C, Goujon C, Bacia M, et al. Magnetic and crystal structures of $BiCrO_3$. Solid State Sci. 2010 May;12 (5):660–664.
[9] Colin CV, Perez AG, Bordet P, et al. Symmetry adapted analysis of the magnetic and structural phase diagram of $Bi_{1-x}Y_xCrO_3$. Phys Rev B. 2012 Jun;85:224103.
[10] Niitaka S, Azuma M, Takano M, et al. Crystal structure and dielectric and magnetic properties of $BiCrO_3$ as a ferroelectromagnet. Solid State Ion. 2004 Aug;172(1–4):557–559.
[11] Belik AA, Iikubo S, Kodama K, et al. Neutron powder diffraction study on the crystal and magnetic structures of $BiCoO_3$. Chem Mater. 2006 Feb;18(3):798–803.
[12] Xu YH, Hao XF, Meng J, et al. Electronic and magnetic properties of the monoclinic phase $BiCrO_3$ from first-principles studies. J Phys Condens Matter. 2009 Jun;21:23.
[13] Yu RZ, Hojo H, Watanuki T, et al. Melting of Pb Charge Glass and Simultaneous Pb-Cr Charge Transfer in $PbCrO_3$ as the Origin of Volume Collapse. J Am Chem Soc. 2015 Oct;137(39):12719–12728.
[14] Ogata T, Sakai Y, Yamamoto H, et al. Melting of d_{xy} Orbital Ordering Accompanied by Suppression of Giant Tetragonal Distortion and Insulator-to-Metal Transition in Cr-Substituted $PbVO_3$. Chem Mater. 2019 Feb;31(4):1352–1358.
[15] Izumi F, Momma K. Three-dimensional visualization in powder diffraction. Proc XX Conf Appl Crystallogr, Solid State Phenom. 2007 Dec;130:15–20.
[16] Momma K, Izumi F. VESTA 3 for three-dimensional visualization of crystal, volumetric and morphology data. J Appl Crystallogr. 2011 Dec;44 (6):1272–1276.
[17] Belik AA. Magnetic properties of solid solutions between $BiCrO_3$ and $BiGaO_3$ with perovskite structures. Sci Technol Adv Mater. 2015 Apr;16(2):2.
[18] Yamamoto H, Ogata T, Sakai Y, et al. Stability of Polar Structure in Filling-Controlled Giant Tetragonal Perovskite Oxide $PbVO_3$. Inorg Chem. 2019 Feb;58 (4):2755–2760.
[19] Sugawara F, Iiida S, Syono Y, et al. Magnetic properties and crystal distortions of $BiMnO_3$ and $BiCrO_3$. J Phys Soc Jpn. 1968;25(6):1553-1558.
[20] Belik AA, Tsujii N, Suzuki H, et al. Magnetic properties of bulk $BiCrO_3$ studied with dc and ac magnetization and specific heat. Inorg Chem. 2007 Oct;46 (21):8746–8751. .
[21] Ding J, Yao YG, Kleinman L. Density functional study of weak ferromagnetism in a thick $BiCrO_3$ film. J Appl Phys. 2011 May;109:10.
[22] Cardoso JP, Delmonte D, Gilioli E, et al. Phase Transitions in the Metastable Perovskite Multiferroics $BiCrO_3$ and $BiCr_{0.9}Sc_{0.1}O_3$: a Comparative Study. Inorg Chem. 2020 Jul;59(13):8727–8735.
[23] Whangbo MH, Gordon EE, Xiang H, et al. Prediction of Spin Orientations in Terms of HOMO-LUMO Interactions Using Spin-Orbit Coupling as Perturbation. Acc Chem Res. 2015 Dec;48 (12):3080–3087.
[24] Yamamoto H, Ogata T, Patel S, et al. $Na_{1/2}Bi_{1/2}VO_3$ and $K_{1/2}Bi_{1/2}VO_3$: New Lead-Free Tetragonal Perovskites with Moderate c/a Ratios. Chem Mater. 2018 Oct;30 (19):6728–6736.
[25] Oka K, Yamauchi T, Kanungo S, et al. Experimental and Theoretical Studies of the Metallic Conductivity in Cubic $PbVO_3$ under High Pressure. J Phys Soc Jpn. 2018 Feb;87(2):024801.
[26] Liu ZH, Sakai Y, Yang JY, et al. Sequential Spin State Transition and Intermetallic Charge Transfer in $PbCoO_3$. J Am Chem Soc. 2020 Mar;142(12):5731–5741.
[27] Ishiwata S, Azuma M, Takano M. Pressure-induced metal-insulator transition in $BiNiO_3$. Solid State Ion. 2004 Aug;172(1–4):569–571.